ACS Catalysis

Research Article

Cite This: ACS Catal. 2019, 9, 8213–8223

pubs.acs.org/acscatalysis

Overwhelming the Performance of Single Atoms with Atomic Clusters for Platinum-Catalyzed Hydrogen Evolution

Minghao Sun,[†,▽] Jiapeng Ji,[†,▽] Mingyu Hu,[‡,▽] Mouyi Weng,[‡,▽] Yaping Zhang,[§] Haisheng Yu,[∥] Jiajun Tang,[⊥] Junchao Zheng,[*,#] Zheng Jiang,[*,∥] Feng Pan,[*,‡] Chengdu Liang,[†] and Zhan Lin[*,†,⊥]

[†]Zhejiang Provincial Key Laboratory of Advanced Chemical Engineering Manufacture Technology, College of Chemical and Biological Engineering, Zhejiang University, Hangzhou 310027, P. R. China

[‡]School of Advanced Materials, Peking University, Shenzhen Graduate School, Shenzhen 518055, P. R. China

[§]State Key Laboratory of Environment-Friendly Energy Materials, School of Materials Science and Engineering, Southwest University of Science and Technology, Mianyang 621010, China

[∥]Shanghai Synchrotron Radiation Facility, Shanghai Institute of Applied Physics, Chinese Academy of Sciences, Shanghai 201204, P. R. China

[⊥]School of Chemical Engineering and Light Industry, Guangdong University of Technology, Guangzhou 510006, P. R. China

[#]School of Metallurgy and Environment, Central South University, Changsha 410083, P. R. China

Supporting Information

ABSTRACT: As one of the dominant configurations, platinum (Pt) single atomic catalysts (SACs) have pushed the performance of the hydrogen evolution reaction (HER) to an unprecedented level due to the maximized atomic utilization efficiency of Pt atoms. However, the contribution of atomic clusters, which exist in SACs as well, to the overall catalytic performance is always overlooked, thus limiting further enhancement of the performance of Pt-catalyzed HER. Herein, we report anchoring Pt atomic clusters on N-doped graphene for ultrahigh performance of the HER. Benefiting from optimized electron transfer and larger binding energy between active centers and the substrate, Pt atomic cluster catalysts (ACCs) exhibit higher catalytic activity than their single atomic counterparts after 4000 cycles and more than 16 h for HER in an acid solution. These findings reveal a vast opportunity to enhance the catalytic performance of chemical reactions with noble-metal-based ACCs in the near future.

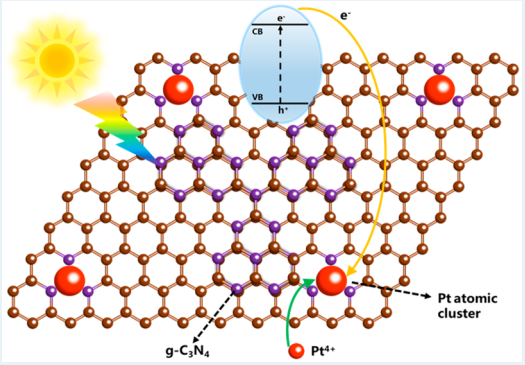

KEYWORDS: *single atomic catalyst, atomic cluster, platinum, graphene, hydrogen evolution*

INTRODUCTION

Hydrogen evolution through the electrocatalytic reduction of water is one of the most promising solution to the problem of fossil fuel depletion. Due to outstanding catalytic activity and stability, platinum (Pt) is currently the best metal catalyst for the electrocatalytic hydrogen evolution reaction (HER).[1,2] However, Pt is intrinsically noble,[3,4] and it is necessary to reduce its loading in catalysts while high catalytic efficiency is maintained.[5,6] Numerous efforts have been devoted to optimize the configurations of active centers in Pt-based catalysts, and commonly used strategies include alloying Pt with transition metals,[7−9] shape-control synthesis,[10,11] and downsizing of active centers.[12,13] Among all catalyst configurations, single-atom catalyst (SAC) represents the lowest limit of particle size while maximum atomic efficiency is maintained.[14] In particular, extremely high catalytic activity and selectivity were explored for noble-metal-based SACs.[15,16] Therefore, the fabrication of Pt-based SACs has become the frontier of Pt-catalyzed HER, which has boosted the performance of electrocatalytic HER to an unprecedented level.[2,17,18]

Currently, the catalytic performance of Pt-based SACs is mainly based on Pt single atoms, which is considered to be the dominant configuration of active centers in Pt-based SACs.[2] In fact, single atoms are not the only configuration of active centers in many SACs, where atomic clusters exist as well.[19] Owing to their extremely high surface free energy, single atoms tend to agglomerate into atomic clusters during synthesis or under working conditions.[20−22] Therefore, the formation of atomic clusters is more energetically favored and thus more

Received: June 3, 2019
Revised: July 20, 2019
Published: July 26, 2019

DOI: 10.1021/acscatal.9b02305
ACS Catal. 2019, 9, 8213−8223

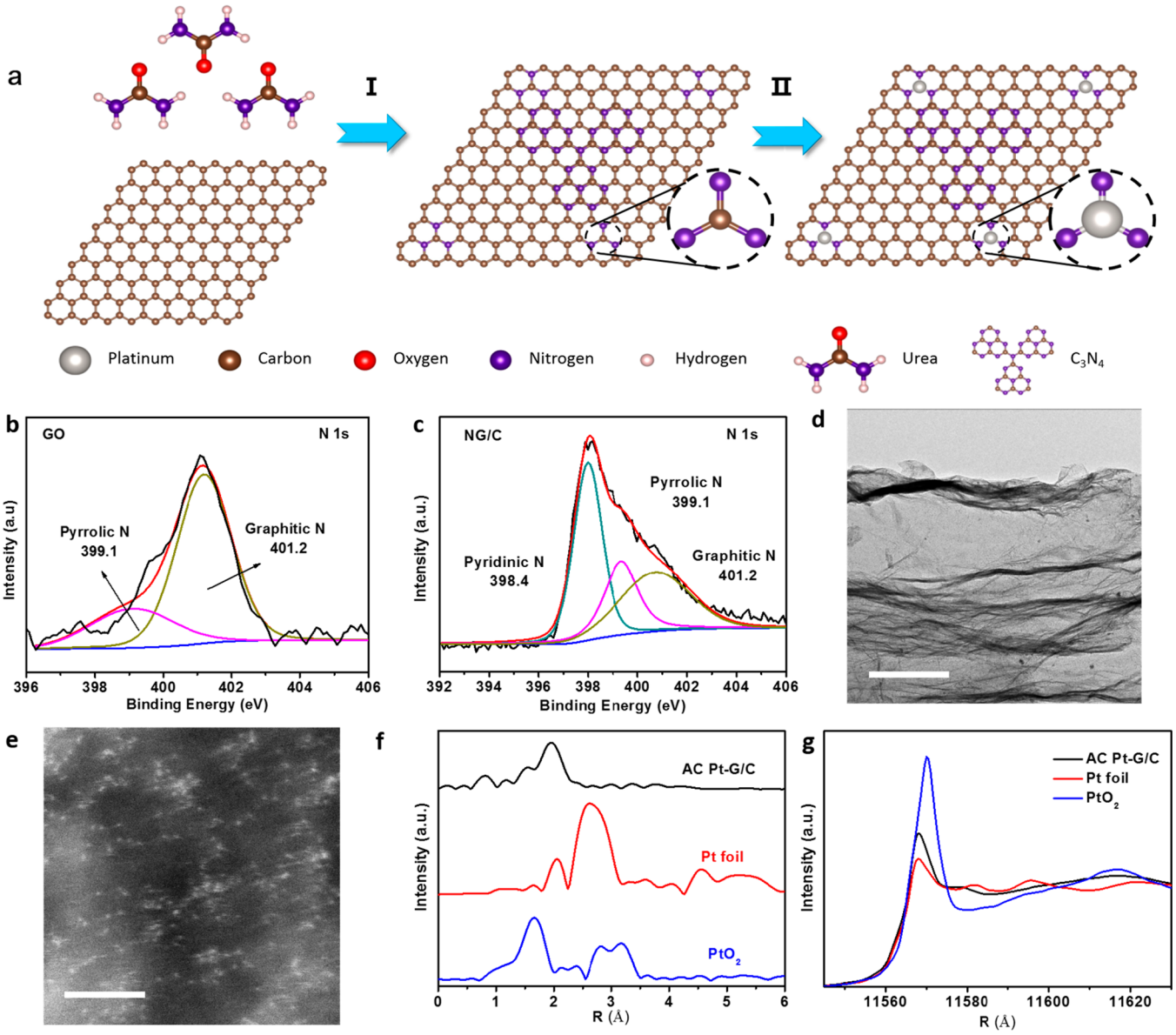

Figure 1. Preparation and characterization of AC Pt-NG/C. (a) Schematic illustration of the main steps involved for the preparation of AC Pt-NG/C. XPS N 1s spectra of (b) GO and (c) NG/C. (d) TEM image of NG/C. (e) ADF-STEM image of AC Pt-NG/C (bright dots in red circles). (f) Normalized XANES spectra at the Pt L_3-edge and (g) k^2-weighted R-space FT spectra from EXAFS of AC Pt-NG/C, Pt foil, and PtO_2. Scale bars: part d, 5 μm; part e, 5 nm.

stable under working conditions than single atoms. Moreover, single atoms do not exhibit their overwhelming advantages in every circumstance, e.g., the catalytic activity of Rh-based atomic clusters toward CO oxidation is 5 times higher than their single-atom counterparts.[23] As such, it is reasonable to speculate that atomic clusters in Pt-based SACs also contribute to the electrocatalytic performance of HER, while catalysts composed of Pt-based atomic clusters could be a promising catalyst configuration to replace state-of-the-art commercial Pt/C catalyst and even push the performance of electrocatalytic HER to a higher level. However, owing to the incapability of current synthesis methods, the comparison of the intrinsic catalytic capability of Pt-based atomic clusters with their single atomic counterparts is rarely reported so far.

In this work, we report Pt-based atomic cluster catalysts (ACCs) loaded on N-doped graphene/graphitic-C_3N_4 (AC Pt-NG/C) via a photodeposition route as a novel configuration of catalytic active centers for HER. The reason why we apply the phrase "atomic clusters" is that we focus on studying the clusters that might exist in traditional SACs. Meanwhile, the word "atomic" best describes the dimension of such clusters. Under visible-light irradiation, graphitic-C_3N_4 (g-C_3N_4) produces electrons,[24] which are separated by N-doped graphene (NG) and transferred on the $\pi-\pi$ conjugation network of NG, allowing for the reduction/anchoring of Pt precursors and the formation of Pt atomic clusters on NG. Comparing with previous works in which only semiconductors are used as substrates to construct SACs via photodeposition,[25,26] a heterogeneous-structured substrate (i.e., NG/g-C_3N_4 composite) is applied in our work, which not only led to improved photoelectric transformation efficiency of g-C_3N_4 under irradiation but also enables optimizing the electronic structure of active catalytic sites in AC Pt-NG/C via tuning the interaction between Pt atomic clusters and

DOI: 10.1021/acscatal.9b02305
ACS Catal. 2019, 9, 8213−8223

substrates (i.e., NG). As proved by DFT calculations, the N content in NG plays a key role in the formation and anchoring of Pt-based atomic cluster, which also contribute to a more desirable adsorption property of hydrogen on Pt-based ACCs than on Pt single atoms or commercial Pt/C catalyst during the catalytic process. As a result, AC Pt-NG/C exhibits high catalytic activity toward HER, exceeding that of commercial 20 wt % Pt/C catalysts by a factor of 21. Meanwhile, AC Pt-NG/C retains extraordinary stability in the chronopotentiometry test for over 16 h and only 5.1 mV losses after 4000 cycles, which is among the best reported, to the best of our knowledge. This work not only provides a novel strategy for constructing a highly efficient and stable catalyst configuration for HER but also promotes large-scale application of Pt-based catalysts in the near future.

RESULTS AND DISCUSSION

Synthesis and Characterizations of AC Pt-NG/C. Owing to different chemical potentials, charge transfers between single atoms and the substrate bring vast opportunities to stabilize metallic single atoms by tuning the structure of the substrate.[27] Among various elements that were applied to modify carbon substrates, N is the most researched and provides not only strong anchoring sites for metallic single atoms but also changes their electronic properties as well.[28] Therefore, in this work we selected NG as the substrate for loading Pt atomic clusters, which was achieved by annealing a GO/urea mixture (step I of Figure 1a).[29] Because the pyrolysis of urea leads to formation of g-C_3N_4,[24] the pyrolysis product is a NG/g-C_3N_4 (NG/C) composite.

N-Doping in NG was first proved by X-ray photoelectron spectroscopy (XPS) measurement. As shown in Figure 1b,c, the N content in NG/C increased violently from 1.2 to 12.05 wt % [Table S1, Supporting Information (SI)] after annealing, most of which was attributed to the increment of pyridinic N. The existence of N in GO is attributed to the oxidation treatment with HNO_3 in the Hummer method.[30] Meanwhile, the decrease of O content and increase of C content in the XPS results (Figure S1 and Table S1, SI) are consistent with the digital images of the products (Figure S2, SI), in which the change of color (from dark brown to black) suggests the restoration of the graphene-like properties in NG,[31] which is favorable for achieving better performance in electrocatalytic HER. Considering that g-C_3N_4 also contributes to the increased N content in the XPS analysis (Figure 1c), we further carried out Raman spectroscopy to confirm N-doping in NG. As shown in Figure S3 (SI), due to the introduction of new structural defects (i.e., N-doping sites) onto the carbon skeleton,[32] the D band (ca. 1350 cm^{-1}) to G band (ca. 1570 cm^{-1}) peak-intensity ratios of the products increased from 0.92 to 1.13 after annealing, while the absence of a 2D peak further demonstrates the defective structure of NG.[33,34] Next, electron microscopy techniques were applied to confirm the existence of g-C_3N_4 in NG/C. Due to the similar layered-structure of g-C_3N_4 and graphene, they tend to become overlapped during annealing.[32] For this reason, NG/C appears darker in certain areas of the transmission electron microscopy (TEM, Figure 1d) image comparing with that of GO (Figure S4a, SI), while the typical wrinkled structure (Figure S4b,c, SI) and large specific surface area of GO were largely retained in NG/C (353 and 282 m^2 g^{-1}, respectively, for GO and NG/C, Figure S5, SI), which is crucial for achieving high loading content and homogeneous anchoring of Pt atomic clusters.[35] The hysteresis in the range of P/P_0 = 0.4−0.9 in the isotherms of NG/C suggests the existence of mesoporous contents, which might be attributed to the formation of g-C_3N_4. Meanwhile, the formation of g-C_3N_4 was further proved by Fourier-transform infrared spectroscopy (FTIR). In Figure S6a (SI), the emergence of new peaks at ca. 800 and 1250 cm^{-1} in the spectra of NG/C is attributed to the breathing vibration of triazine units and the stretching mode of C−N in g-C_3N_4.[30] While in the powder X-ray diffraction (XRD) patterns (Figure S6b, SI), the typical interlayer-stacking of aromatic segments peak at 27.5° is indexed as (002) of g-C_3N_4.[36] On the basis of the above, we conclude that NG/C is a highly N-doped material, while the g-C_3N_4 on NG/C is favorable for the subsequent synthesis of AC Pt-NG/C via photodeposition.

For the synthesis of AC Pt-NG/C, an aqueous dispersion of NG/C containing a target amount of H_2PtCl_6 was exposed to visible-light irradiation (step II of Figure 1a). The absorption edge of the aqueous mixture is ca. 460 nm, as determined by the UV−vis diffuse reflectance spectra (DRS, Figure S7a, SI), which is identical to that of g-C_3N_4.[37] After irradiation, the peak-intensity ratio of AC Pt-NG/C further decreased to 0.98 compared with that of NG in the Raman spectra (Figure S7b, SI), and this is attributed to the elimination of oxygen functional groups in NG by the photodriven electrons, as proved by the XPS results (Figure S8a, SI).[31] The carbon and nitrogen contents are almost consistent (Figure S8b,c, SI), which confirms that NG could separate electrons from g-C_3N_4 under irradiation and is consistent with the established role of g-C_3N_4 as a photoelectric transformation mediator. The similar FTIR spectra of AC Pt-NG/C and NG/C (see Figure S6a, SI) suggest that the major fraction of the photogenerated electrons is consumed in the reduction of Pt precursors or dissipated as heat rather than in the elimination of oxygen functional groups.

Due to the Pt content in AC Pt-NG/C being low, no Pt nanoparticles (NPs) could be observed in the SEM (Figure S9a, SI) and TEM (Figure S9b, SI) images of AC Pt-NG/C. Particularly, the absence of Pt NPs even in the high-resolution transmission electron microscopy (HRTEM, Figure S9c, SI) images of AC Pt-NG/C should be noted, and no characteristic peaks of Pt crystals could be observed in the XRD patterns of AC Pt-NG/C (Figure S10, SI), which suggests an extremely fine dispersion of Pt in AC Pt-NG/C. Therefore, we further resorted to aberration-corrected annular dark-field scanning transmission electron microscopy (ADF-STEM) to investigate the dispersion state of Pt in AC Pt-NG/C. As shown in Figure 1e, taking into consideration the sharp *Z*-contrast between metallic materials and carbon matrix, we attribute uniformly distributed bright dots (with diameters of ca. 0.5 nm) to small Pt clusters in AC Pt-NG/C,[2] which exhibits atomically dispersed features and amounts to 2.0 wt % in AC Pt-NG/C according to the inductively coupled plasma-optical emission spectrometry (ICP-OES) analysis. Energy dispersive spectroscopy (EDS) mapping (Figure S11a−d, SI) proves that only trace amount of Pt (Figure S11b, SI) could be detected on the surface of AC Pt-NG/C, which is consistent with the ICP-OES results. Meanwhile, nitrogen (Figure S11c, SI) and carbon (Figure S11d, SI) elements are distributed homogeneously all over the surface of AC Pt-NG/C, further proving that NG/C is a highly N-doped substrate.

Owing to the surface free energy of single atoms being extremely high, causing agglomeration during processing, a decreased loading content of metallic active materials in SACs will lead to higher atomic ratio of single atoms in the active

DOI: 10.1021/acscatal.9b02305
ACS Catal. 2019, 9, 8213−8223

centers.[38] In this work, further increasing the loading content of Pt (e.g., 3 wt %) in AC Pt-NG/C generates Pt nanoparticles in the products (Figure S12a, SI). Therefore, to compare the efficacy of atomic clusters with single atoms, we halved the content of Pt in AC Pt-NG/C, with other synthesis conditions being kept equal, to prepare another catalyst; the product is denoted as 1-Pt-NG/C. As shown in Figure S12b (SI), no Pt nanoparticles are detected in the ADF-STEM image of 1-Pt-NG/C. Theoretically, the atomic ratio of single atoms in the active centers of 1-Pt-NG/C should be higher than that of AC Pt-NG/C. In the BET tests (Figure S13, SI), AC Pt-NG/C (272 m^2 g^{-1}) and 1-Pt-NG/C (263 m^2 g^{-1}) demonstrate similar specific surface areas, and the mesoporous feature of NG/C is retained in both catalysts. Size distributions of Pt particles in AC Pt-NG/C and 1-Pt-NG/C are calculated on the basis of the ADF-STEM images [see Figures 1e and S12b (SI)], and the results (Figure S14, SI) reveal that the average sizes of Pt particles in AC Pt-NG/C (ca. 0.61 nm) is larger than that of 1-Pt-NG/C (ca. 0.54 nm), suggesting that the latter contains a higher ratio of single atoms in active centers. Comparing with previous reports of Pt-based SACs,[38] the average sizes of Pt particles in this work are relatively smaller, and this could be attributed to the mild synthesis conditions of photodeposition,[39] which favors a homogeneous distribution of active centers in the products.

To achieve deeper insights into the particle size distribution of the catalysts, a CO chemisorption test is applied to investigate the ratio of surface Pt atoms in AC Pt-NG/C and 1-Pt-NG/C. Generally, as the size of nanoparticle decreases, more atoms will be exposed to the surface, which leads to a higher CO adsorption capacity of the nanoparticles. In this work, the CO/metal mole ratio ($R_{CO/metal}$) of AC Pt-NG/C and 1-Pt-NG/C is 0.71 and 0.49, respectively, suggesting that the average size of Pt particles in AC Pt-NG/C is larger, which is consistent with the ADF-STEM results. However, contrary to the expectation that most of the Pt atoms in the catalysts should be exposed to the surface, because the average sizes of Pt particles are extremely small,[38] it is surprising to find that a large fraction of Pt atoms in the catalysts do not adsorb CO, especially for 1-Pt-NG/C. According to the work of Bulushev et al., CO adsorbs strongly on the surface of Pt-group metals. However, back-donation of metal d-electrons to the π^* antibonding orbital of CO is greatly dampened in the case of metal ions, which weakens the strength of the CO−metal bond. As a result, the adsorption energy of CO on positively charged Pt particles is much weaker compared to that of a negatively charged or neutral particle,[40] which deteriorates the adsorptive capability of some Pt atoms toward CO. On the basis of the above, we speculate that some Pt atoms in AC Pt-NG/C and 1-Pt-NG/C carry positive charges, which leads to the deviation of surface Pt atomic ratios in the catalysts from expectation and is proved by the XPS tests. As shown in the Pt 4f spectrum (Figure S15a,b, SI), both AC Pt-NG/C and 1-Pt-NG/C contain considerable amounts of Pt^{2+} in the active centers. Meanwhile, the Pt^0/Pt^{2+} ratio of AC Pt-NG/C (ca. 1.25) is higher than that of 1-Pt-NG/C (ca. 1.08), suggesting that a larger fraction of Pt atoms in 1-Pt-NG/C has direct contact with the substrates compared with AC Pt-NG/C, which carries positive charges due to the electronegativity of Pt being much smaller than that of the light atoms (e.g., C, N, O) in NG/C substrates and does not adsorb CO strongly, as suggested by the results of CO chemisorption tests. The small peaks located at ca. 74 and 77.5 eV of the fitted spectra might be attributed to the Pt^{4+} coordinated with O atoms in the graphene substrates or the PtO_2 contents,[41] since the electronegativity of O (3.5) is larger than those of C (2.5) and N (3.0).[42] However, it is unlikely that the Pt^{4+} state is related to the $(PtCl_6)^{2-}$ ions in the precursors, for we have washed the catalysts thoroughly before using, and the corresponding peaks of Cl are extremely weak in the full XPS spectra of both specimens (Figure S15c,d, SI). To sum up, the CO chemisorption tests and XPS results prove that the interaction between the Pt active centers (e.g., Pt atomic clusters and Pt single atoms) and NG/C substrates is strong; moreover, AC Pt-NG/C possesses a higher ratio of Pt atomic clusters in active centers than 1-Pt-NG/C.

X-ray absorption of fine structure (XAFS) measurement is a powerful technique that gives structural information on the catalysts at the atomic scale, which could be divided into the X-ray absorption near-edge structure (XANES) region and extended X-ray absorption fine structure (EXAFS) region. In this work, the white-line (WL) peak of AC Pt-NG/C is located between those of Pt foil and PtO_2 (Figure 1f), suggesting that some Pt atoms carry positive charges, which is consistent with the XPS results (see Figure S15a, SI). In the Fourier transforms of EXAFS (i.e., *R*-space, Figure 1g),[43] the only prominent peak at ca. 2.0 Å in the spectra of AC Pt-NG/C is related to Pt−N/O/C contributions, suggesting that no Pt NPs were formed in AC Pt-NG/C.[44] Albeit the difference in Pt contents, 1-Pt-NG/C possesses similar threshold energy (E_0) and maximum energy (E_{peak}) as AC Pt-NG/C in the XANES measurement (Figure S16a, SI),[45] which is consistent with previous works, yet the reason is still unknown.[2] Meanwhile, the peak at ca. 2.0 Å in the Fourier transforms of EXAFS of 1-Pt-NG/C is sharper comparing with that of AC Pt-NG/C (Figure S16b, SI), and this might be attributed to the ratio of Pt single atoms being higher in the active centers of 1-Pt-NG/C, which leads to more prominent "single-atomic" features of the catalyst. It is interesting to note that the strong peak at 2.6 Å in the FT-EXAFS spectra of Pt foil is absent in those of AC Pt-NG/C and 1-Pt-NG/C. As proved by previous works,[2] the significant Pt−Pt peak in FT-EXAFS spectra will become dampened and shifted to higher positions in the case of Pt clusters; meanwhile, the intensity of the Pt−Pt peak becomes even weaker as the size of Pt cluster reduces, which indicates that FT-EXAFS is sensitive to the size of atomic clusters. In our work, the diameters of Pt atomic clusters are extremely small, as proved by ADF-STEM images [see Figures 1e and S12b (SI)] and DFT calculations (see details below in Figure 3a), and both contribute to the very small peak at ca. 2.6 Å in FT-EXAFS spectra of AC Pt-NG/C. Therefore, it is reasonable to conclude that a large fraction of the Pt species in AC Pt-NG/C exhibit the typical features of ACCs.

Electrocatalytic Measurements. We first carried out the electrochemical impedance spectroscopy (EIS) measurements to gain more information about the electrolytes. In Figure S17 (SI), the intersection of the semicircle and real axis in the high-frequency region of Nyquist plots represents the resistance of electrolyte solution (R_s).[46,47] In this work, R_s is kept consistent (ca. 8 Ω), covering both HER and non-HER conditions at room temperature, thus making the results of subsequent tests more convincing.

To make the electrochemical results of AC Pt-NG/C and 1-Pt-NG/C more convincing, commercial 20 wt % Pt/C catalysts is applied as a control sample during electrochemical tests (for more details of the 20 wt % Pt/C catalysts, see the

DOI: 10.1021/acscatal.9b02305
ACS Catal. 2019, 9, 8213−8223

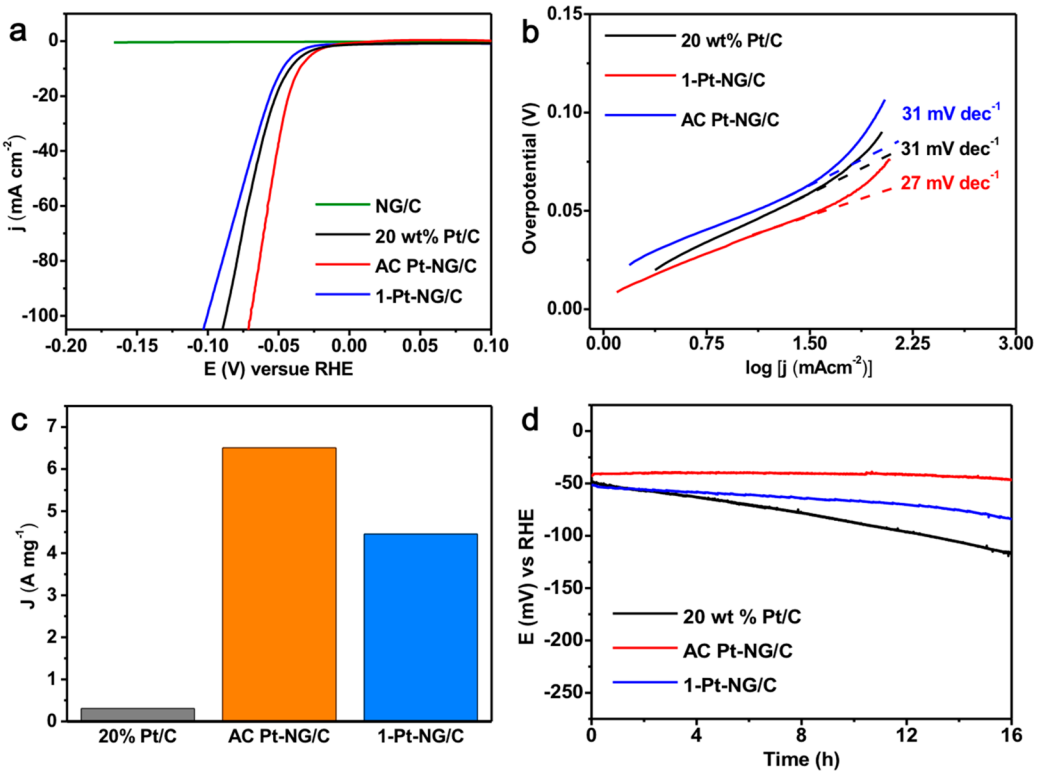

Figure 2. Electrocatalytic performance of the catalysts. (a) Electrochemical performances of the catalysts in LSV measurements. (b) Tafel plots obtained from the polarization curves in part a. (c) Mass activity of different catalysts at the potential of −50 mV (vs RHE) derived from the LSV curves in part a. (d) Chronopotentiometry curves (without IR compensation) of different catalysts.

Experimental Section). In the LSV tests, AC Pt-NG/C exhibits smaller overpotential (η, 35.28 mV, Table S2, SI) than 1-Pt-NG/C (47.20 mV), commercial 20 wt % Pt/C catalysts (42.03 mV), and state-of-the-art Pt-based SACs for HER (Table S3, SI) at a current density of 10 mA cm^{-2} (Figure 2a), suggesting the high catalytic activity of AC Pt-NG/C toward HER. Considering that a higher Pt content may enhance the HER catalytic performance,[2] Tafel and turnover frequency (TOF) analysis was performed to gain further insight into the intrinsic catalytic activity of each Pt atom in the catalysts. As shown in Figure 2b, the Tafel slope value of 20 wt % Pt/C is identical to that of 1-Pt-NG/C (31 mV dec^{-1}) and is consistent with those values in published reports,[2] while AC Pt-NG/C exhibits smaller Tafel slopes of 27 mV dec^{-1} under the same conditions, suggesting that the reaction was catalyzed through a Volmer−Tafel process.[48,49] Exchange current densities (j_0) were obtained from the Tafel plots by an extrapolation method.[50] The j_0 value of AC Pt-NG/C was calculated to be 0.520 mA cm^{-2}, which is larger than that of 20 wt % Pt/C (0.513 mA cm^{-2}) and 1-Pt-NG/C (0.240 mA cm^{-2}), suggesting the superior catalytic activity of Pt atoms in AC Pt-NG/C.

The TOF value is a direct criterion of the catalytic activity of a single active site.[51] In this work, the TOF values of the specimens were obtained at thermodynamic potential (e.g., 0 V vs RHE) according to the exchange current densities, among which the TOF value of AC Pt-NG/C was calculated to be 0.0927 S^{-1}, which was an order of magnitude higher than that of 20 wt % Pt/C (0.00915 S^{-1}) and much higher than that of NP Pt-NG/C (0.0854 S^{-1}). In most cases, a decreased loading content of active materials will lead to a higher TOF value of a catalyst;[52] therefore, we were surprised to find that AC Pt-NG/C with higher loading content of Pt than 1-Pt-NG/C exhibited a higher TOF value, which suggests that Pt atomic clusters possess better HER catalytic capability than Pt single atoms. For a better understanding of the HER catalytic activity, the areal current density of AC Pt-NG/C is compared with that of commercial Pt/C catalysts 1-Pt-NG/C and state-of-the-art Pt-based SACs for HER (Figure S18 and Tables S3 and S4, SI) at η = 50 mV versus RHE, at which AC Pt-NG/C presents the highest value (36.9 mA cm^{-2}). The results are more striking when current densities are normalized to Pt mass. As shown in Table S4 (SI), the mass current density of AC Pt-NG/C reached 6.508 A mg^{-1} at η = 0.05 V (vs RHE), which is 1.46 and 21.06 times higher than that of 1-Pt-NG/C (4.456 A mg^{-1}) and 20 wt % Pt/C (0.309 A mg^{-1}), respectively (Figure 2c). These results confirm the excellent intrinsic catalytic activity of Pt atomic clusters in AC Pt-NG/C.

To achieve further insight into the catalytic activity of Pt atomic clusters and Pt single atoms, we construct two more specimens by further decreasing the loading content of Pt in the catalysts, namely, 0.5-Pt-NG/C and 0.25-Pt-NG/C. As shown in Figure S19a,b (SI), no Pt particles up to 1 nm can be observed in the ADF-STEM images of 0.5-Pt-NG/C and 0.25-Pt-NG/C, while their Pt^0/Pt^{2+} ratios (0.29 and 0.17, respectively, for 0.5-Pt-NG/C and 0.25-Pt-NG/C; see Figure S19c,d, SI) decrease consecutively compared with that of 1-Pt-NG/C (1.08), suggesting that the ratios of Pt atomic clusters in the catalysts decrease in the order of 1-Pt-NG/C > 0.5-Pt-NG/C > 0.25-Pt-NG/C. In the LSV measurements (Figure S20a, SI), the 0.5-Pt-NG/C (66.10 mV) and 0.25-Pt-NG/C (95.75 mV) catalysts exhibit larger η than 1-Pt-NG/C (47.20 mV) at a current density of 10 mA cm^{-2}, suggesting that the catalytic activity of 1-Pt-NG/C is higher toward HER.

DOI: 10.1021/acscatal.9b02305
ACS Catal. 2019, 9, 8213−8223

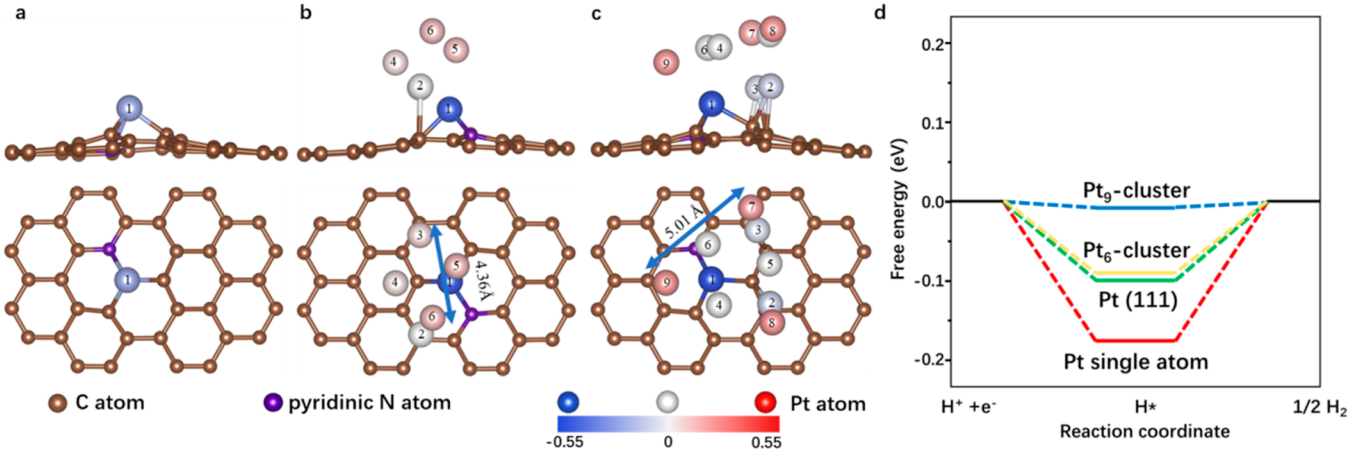

Figure 3. DFT calculation for the energetics of Pt atom agglomeration to promote the HER activity. Energy favorable adsorption structures of (a) Pt single atom, (b) Pt_6-cluster, and (c) Pt_9-cluster on pyridinic N graphene substrate were obtained by the PSO algorithm. Their corresponding Bader charges were analyzed to distinguish Pt atoms using gradient colors. The profiles of each atom are shown at the bottom. (d) Calculated free energy diagram for hydrogen evolution at equilibrium (applied potential $U = 0$) with the above different catalyst configurations. The red, yellow, and blue lines represent the calculated ΔG_{H^*} for Pt single atom, Pt_6-cluster, and Pt_9-cluster, respectively, compared with Pt(111) slab (green line).

Meanwhile, the areal current densities and mass activities of the catalysts increase in the order of 0.25-Pt-NG/C < 0.5-Pt-NG/C < 1-Pt-NG/C (Figure S20b,c, SI), confirming that the Pt atomic clusters are more active than their single atomic counterparts. It should be noted that the differences in mass activity of 1-, 0.5-, and 0.25-Pt-NG/C are small (Figure S20c, SI). Generally, for Pt-based SACs with carbonaceous substrates, Pt single atom is the major configuration of active centers when the loading content of Pt is below 1 wt %,[2,38] which should be the same case for 1-, 0.5-, and 0.25-Pt-NG/C in this work, because the mild synthesis conditions of photodeposition are favorable to achieve uniform distribution of active centers.[39] Therefore, albeit the large differences in Pt loading content and areal current densities, it is reasonable that the Pt single atoms in 1-, 0.5-, and 0.25-Pt-NG/C exhibit similar mass activities. To conclude, the above results are enough to back up the conclusion that Pt atomic clusters are more active than their single atomic counterparts toward HER.

Furthermore, long-term cycling tests were carried out to evaluate the stability of AC Pt-NG/C under working conditions. As shown in Figure S21a (SI), after 4000 cyclic voltammetry (CV) cycles, the η of 20 wt % Pt/C shifted negatively by more than 56.4 mV at a current density of 10 mA cm^{-2}, suggesting a significant decrease in catalytic activity, which may be attributed to the weak interaction between Pt NPs and the arbon substrate, thus leading to serious detachment and agglomeration of Pt NPs during the tests.[53] In contrast, the polarization curve of AC Pt-NG/C exhibited negligible potential decay after 4000 cycles (Figure S21b, SI) and only lost 5.1 mV after 4000 cycles, which is an order of magnitude smaller than that of 20 wt % Pt/C and much lower than that of 1-Pt-NG/C (8.1 mV, Figure S21c, SI). Moreover, AC Pt-NG/C exhibits an overwhelming advantage over 20 wt % Pt/C in the chronopotentiometry test. As shown in Figure 2d, the catalytic activity of 20 wt % Pt/C and 1-Pt-NG/C kept fading throughout the test, which lost 73 and 34 mV, respectively, after 16 h. Meanwhile, AC Pt-NG/C stayed highly active with rare attenuation under the same conditions (5 mV). The above results confirmed that the stability of AC Pt-NG/C is among the best reported for Pt-based SACs (Table S5, SI). It is important to note that the higher catalytic stability of AC Pt-NG/C compared with 1-Pt-NG/C proves that Pt atomic clusters are more stable than Pt single atoms under the working conditions of HER. Therefore, more work should be devoted to construct Pt-based ACCs featuring higher ratios and more uniform distribution of Pt atomic clusters.

Theoretical Calculations and Mechanism Discussion. Owing to the electrical conductivities of semiconductors being low, most of the electron (e^-)/hole (h^+) pairs generated under irradiation are recombined immediately after generation, resulting in the low photoelectric transformation efficiency (PTE) of the semiconductors.[39] Compositing photoreactive semiconductors with electrical conductors (e.g., graphene or carbon nanotubes) is an efficient strategy that improves the PTE of semiconductors by separating the as-generated e^- from h^+ as soon as they are generated under irradiation.[54] As a result, photogenerated electrons are shuttled and transferred on electrical conductors, which binds and reduces redox mediators at locations on electrical conductors distinct from anchoring sites of semiconductors, which has already been proved by previous works.[55] Therefore, in this work, it is reasonable to conclude that Pt catalytic active centers locate at sites distinct from g-C_3N_4 on NG. More importantly, owing to the electrical conductivity of g-C_3N_4 being extremely low,[37] Pt catalytic active centers loaded on g-C_3N_4 will not contribute to the electrocatalytic performance of catalysts at the working conditions of this work.

On the basis of the above, density functional theory (DFT) calculations were carried out to obtain atomic-scale insight into the catalytic effect of AC Pt-NG/C. First of all, we tried to clarify the most energetically favorable adsorption site for Pt single atoms on NG. All the inequivalent Pt-adsorption configurations (Figure S22a–d, SI) around N atoms (namely, pyridinic, graphitic, and pyrrolic N atoms in Figure S22e) and pristine graphene were considered. The adsorption energies (E_a) were calculated by the following equation

$$E_a = E_{Pt/sub} - E_{Pt} - E_{sub} \quad (1)$$

where $E_{Pt/sub}$ is the total energy of the substrate (i.e., all N configurations in NG, or pristine graphene) with an adsorbed Pt single atom, E_{Pt} is the energy of a Pt single atom referred to

DOI: 10.1021/acscatal.9b02305
ACS Catal. 2019, 9, 8213–8223

its bulk metal, and E_{sub} is the energy of the substrate. According to the calculated results (Table S6, SI), Pt single atoms are more prone to adsorbing on pyridinic N comparing with other substrates, with the largest adsorption energy of −5.173 eV (on site III, Figure S22a, SI). The Bader charge analysis suggests that 0.252 e^- is transferred from the adsorbed Pt single atom to the pyridinic N, confirming that site III in Figure S22a (SI) is the most energy favorable adsorption site for a Pt single atom. We also proved that pyrrolic N tends to transform into pyridinic N (Figure S23, SI); this is consistent with the XPS results in Figure 1c, which suggest a vast increment of pyridinic N after annealing. Besides, as shown in Figure S24 (SI), the Pt atom adsorbed on site II of pyrrole N splits the substrate, which has a negative effect on base structures. On the basis of the above experimental and DFT calculation results, pyridinic N substrate was selected to investigate the adsorption structure of Pt clusters.

In order to predict the adsorption structures more efficiently and investigate the catalytic performance of Pt clusters on N-doped graphene, the structure of Pt clusters (n = 4−12) and their adsorption structures on the pyridinic N in NG were predicted on the basis of the particle swarm optimization (PSO) algorithm within the evolutionary scheme using the CALYPSO package.[56,57] The adsorption structures of clusters consisting of six and nine Pt atoms (denoted as Pt_6-cluster and Pt_9-cluster, respectively) were investigated and compared according to the size range of bright dots in the ADF-STEM image (Figure S14, SI). As shown in Figure 3a−c, Bader charge analysis was also conducted to clarify charge transfer and total electronic charge of adsorbed Pt atoms (see details in Table S7, SI), before hydrogen adsorption. The results reveal that Pt atoms present various degrees of electron-deficient and electron-rich phenomenon, which were described by gradient colors. In the case of Pt_6- and Pt_9-clusters, the Pt atoms (blue atoms in Figures S25 and S26, SI) which are directly bonded to the pyridinic N have the largest charge transfer (0.500 e^- and 0.516 e^-, respectively, for Pt_6-cluster and Pt_9-cluster), implying their stronger bonding energy to the substrate than that of Pt single atom (0.252 e^-), which contributes to the anchoring of the Pt atomic clusters. Meanwhile, the Pt atoms in the top layer of the Pt_9-cluster structure can be classified by the amount of charge transfer; i.e., the neutral Pt atoms [gray atoms, Pt(4), Pt(5) and Pt(6) in Figure 3c] undego almost no charge transfer while the other three Pt atoms [light red atoms, Pt(7), Pt(8), and Pt(9) in Figure 3c] are electron-rich within the Bader volume. Both kinds of Pt atoms construct bridge sites in the Pt_9-cluster synergistically, and this configuration is expected to promote a synergistic catalytic effect, which might be the primary reason for the enhanced HER activity of the Pt_9-cluster.

To gain further insight into the HER catalytic capability of AC Pt-NG/C, the Gibbs free energies (ΔG_{H^*}) of atomic hydrogen adsorption, which is a reasonable descriptor of the catalytic ability of a material toward HER, were calculated for various Pt-based active centers and the majority of inequivalent catalytic sites (Figure S25−S27) by the following equation

$$\Delta G_{H^*}^{SAC} = \Delta E_{H^*}^{SAC} - \Delta E_{H^*}^{Pt} + \Delta G_{H^*}^{Pt} \quad (2)$$

where $\Delta E_{H^*}^{SAC}$ and $\Delta E_{H^*}^{Pt}$ are the hydrogen chemisorption energies of SAC surface and Pt(111), respectively, and $\Delta G_{H^*}^{SAC}$ and $\Delta G_{H^*}^{Pt}$ are the Gibbs free energies of atomic hydrogen adsorption on SAC surface and Pt(111) slab. On the basis of the theory proposed by Nørskov and co-workers, the desirable ΔG_{H^*} value of a HER catalyst should be around 0.00 eV and the Gibbs free energy of Pt(111) on the fcc site was calculated previously (−0.1 eV).[58] Comparing with other catalytic centers, the calculated ΔG_{H^*} values of bridge sites between neutral and electron-rich atoms in Pt_9-cluster (i.e., the adsorption sites in Figures S25a,b and S26a−c) are closer to 0.00 eV, suggesting its better HER catalytic capability in the view of the thermochemistry.[58] As illustrated in Figures 3d and 4, the optimal ΔG_{H^*} values of the Pt single atom, Pt_6-cluster, and Pt_9-cluster configurations are −0.176, −0.096, and −0.008 eV, respectively, suggesting that the capability of various Pt active centers to catalyze HER is in the order Pt_9-cluster > Pt_6-cluster > Pt slab(111) > Pt single atom. It should be noted that the ΔG_{H^*} value of a Pt single atom adsorbed on pyridinic N is the lowest, which means that a hydrogen atom is bonded too strongly on the substrate, thus decreasing the efficiency of hydrogen adsorption and release.[59] To sum up, the calculated results are consistent with the experimental results, which also proved the higher intrinsic activity of Pt atoms in the atomic clusters comparing with those in their single atomic form.

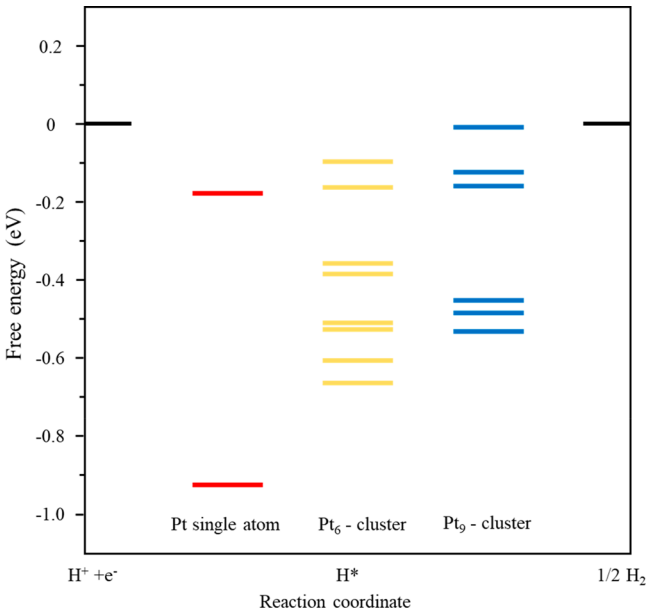

Figure 4. Free energy diagram for hydrogen evolution at equilibrium. The red, yellow, and blue lines represent the calculated ΔG_{H^*} of inequivalent catalytic sites for Pt single atom, Pt_6-cluster, and Pt_9-cluster, respectively.

CONCLUSIONS

In conclusion, we demonstrate that Pt-based ACCs, as a promising type of catalyst configuration, is highly active toward HER, which not only exhibit higher catalytic activity than their single atomic counterparts and commercial 20 wt % Pt/C catalysts but also remain highly active after 4000 catalytic cycles or after 16 h in the chronopotentiometry tests. DFT calculation results reveal that the pyridinic N contents in the substrate of the Pt-based ACCs play a key role in stabilizing the Pt atomic clusters, which also promotes charge transfer between the Pt atomic cluster and the substrates, leading to optimized hydrogen adsorption and releasing properties on the catalyst surface. This work not only provides an efficient strategy for constructing highly active catalyst configurations for HER but also brings vast opportunities to enhance the

DOI: 10.1021/acscatal.9b02305
ACS Catal. 2019, 9, 8213−8223

catalytic performance of various chemical reactions, such as photocatalysis and organic synthesis.

EXPERIMENTAL SECTION

Materials. Analytical-grade urea and ethanol were obtained from Shanghai Chemical Reagents. Chloroplatinic acid (H_2PtCl_6, 99.995%) and Nafion (5 wt % in a mixture of lower aliphatic alcohol and water) were acquired from Sigma-Aldrich. Pt/C (20 wt %) catalysts with a specific surface area of 200.1 $m^2\ g^{-2}$ (Figure S28a, SI) were acquired from Macklin. Meanwhile, the pore volume is 0.427 $cm^3\ g^{-1}$ and the average pore diameter is 12.8 nm (Figure S28b, SI). The Pt nanoparticles are uniformly distributed on the catalyst surface (Figure S28c, SI). The average size of the Pt nanoparticles is calculated to be 3.32 nm on the basis of the HRTEM results (Figure S28d, SI). Graphite rod was obtained from Alfa Aesar (99.9995%). All of the chemicals used in this experiment were of analytical grade and used without further purification. Deionized (DI) water (18.2 MΩ at 25 °C) was obtained from a Milli-Q System (Millipore, Billerica, MA).

Synthesis of NG/C Composite. NG/C was prepared according to previous reports,[24] in which the mass ratio of NG to g-C_3N_4 was 3:2. In a typical procedure, graphene oxide (GO) solution (3 mg mL^{-1}) was prepared by a modified Hummer method.[1] Subsequently, 1.2 g of urea (NH_2CONH_2) was added into 6 mL of GO solution under vigorous stirring until fully dissolved. Then, the mixture was dehydrated at 60 °C in a vacuum oven for 12 h. The as-obtained GO/urea mixture was loaded into the center of a tube furnace (calibrated using a k-type thermocouple probe). After flushing the tube with Ar (150 sccm) for 30 min, the temperature was ramped at 10 °C min^{-1} until 600 °C and maintained for 2 h under continuous Ar flow, followed by naturally cooling to room temperature. The final product of NG/C composite was collected and washed three times with DI water under sonication.

Synthesis of AC Pt-NG/C. For the preparation of all catalysts in this work, UV irradiation was provided by a xenon-lamp parallel light source system (Beijing Perfectlight Science & Technology Co. Ltd., CHF-XM-500W) operating at a current of 15 A, with the distance between liquid surface and the light source being kept at 5 cm. In a typical synthesis, 30 mg of NG/C composite was dispersed in 20 mL of deionized water under sonication for 5 min. Then, a H_2PtCl_6 aqueous solution (2 mg mL^{-1}, 0.796 mL) was injected into the above aqueous dispersion under vigorous stirring. The mass ratio of Pt to NG/C is 2 wt % (for the synthesis of 1-Pt-NG/C, 0.5-Pt-NG/C, and 0.25-Pt-NG/C, the mass ratio of Pt to NG/C is 1, 0.5, and 0.25 wt %, respectively). Subsequently, the mixture was exposed to visible light irradiation under continuous stirring for 6 h. Finally, the products were collected and washed three times with DI water under sonication followed by dehydrating in a vacuum oven.

Characterizations. Visible light was provided by a Xenon-lamp parallel light source system (Beijing Perfectlight Science & Technology Co. Ltd., CHF-XM-500W). XRD spectra were obtained at room temperature using an X'Pert PRO (PANalytical, Netherlands) instrument with Cu Ka radiation. Chemisorption of CO was performed on a AutoChem1 II 2920 (Micromeritics) in pulse mode, using He as the carrier gas. Raman spectroscopy was conducted using a laser confocal Raman microspectroscope (LabRAM HR Evolution, Horiba Jobin Yvon). FTIR spectra were recorded on FT-IR TENSOR 27 (Bruker) equipment using a KBr pellet in the range of 800−4000 cm^{-1}. UV−vis spectra were measured by a UV3600 (Shimadzu). XPS analyses were performed on an Escalab 250Xi XPS system with an Al Kα (1486.6 eV) source. ICP-OES measurements were carried out with an Optima 5300DV system (PerkinElmer). XAFS measurements were performed on the BL14W1 beamline at the Shanghai Synchrotron Radiation Facility (Shanghai Institute of Applied Physics), operated at 3.5 GeV with injection currents of 140−210 mA. A Si(111) double-crystal monochromator was used to reduce the harmonic component of the monochrome beam. Pt foil and PtO_2 were used as reference samples and measured in the transmission mode. ADF-STEM images were obtained on a FEI TITAN Chemi STEM equipped with a CEOS (Heidelburg, Germany) probe corrector, operating at 200 kV. Transmission electron microscopy (TEM) and high-resolution transmission electron microscopy (HRTEM) were conducted using a JEM-2100F field-emission TEM. Scanning electron microscopy (SEM) was performed with a Hitachi S-4800 field emission scanning electron microscope (FE-SEM) (5 kV) equipped with an energy-dispersive X-ray (EDX) spectroscope. The Brunauer−Emmett−Teller (BET) specific surface area of the samples was measured by nitrogen adsorption at 77 K on a surface area and porosity analyzer (Micrometrics ASAP 2020). Pore size distribution plots were derived from the adsorption branch of the isotherm based on density functional theory (DFT) calculations. Cyclic voltammetry (CV), linear sweep voltammetry (LSV), and electrochemical impedance spectroscopy (EIS) were performed on a CHI660E electrochemical workstation (CH Instruments) equipped with a rotating disk electrode (AFMSRCE, Pine Instruments).

Electrochemical Measurements. Electrochemical measurements were carried out in a three-electrode system in a H_2SO_4 electrolyte (0.5 M). All the measured potentials were calibrated to the reversible hydrogen electrode (RHE) using the following equation: $E_{RHE} = E_{Hg/Hg_2SO_4} + 0.64\ V + 0.0592\ pH$.[17] A glassy carbon rotating-disk electrode with a diameter of 3 mm (Pine Instruments), Hg/Hg_2SO_4 electrode (saturated K_2SO_4 aqueous solution, 0.64 V RHE), and graphite rod (Alfa Aesar, 99.9995%) were applied as the working electrode, reference electrode, and counter electrode, respectively. For the preparation of the working electrode, 2 mg of the catalyst and 12 μL of Nafion solution was first dispersed in 1 mL of water/ethanol (v:v = 1:9) solution under sonication. The above dispersion (10 μL) was then loaded onto a glassy carbon electrode and dried naturally at ambient environment, and the loading amount of catalyst was ca. 0.283 mg cm^{-2}. LSV measurement was performed with a scan rate of 5 mV s^{-1} and a rotating speed of 1600 rpm. The polarization curves were corrected with 95% IR compensation (IR corrected).[49] Areal/mass current densities were obtained by normalizing the current to the geometric area of the electrode and Pt mass, respectively. Electrochemical impedance spectroscopy (EIS) was conducted in a frequency range from 0.1 to 100 000 Hz at an overpotential of 200 mV (versus RHE) to obtain the solution resistance (R_s). All data presented were corrected with the solution resistance R_s.[50,60] The number of active sites and turnover frequency (TOF) of the catalysts were calculated according to previous reports.[49,52]

DFT Calculations. All first-principles calculations were performed by the Vienna Ab-initio Simulation Package

DOI: 10.1021/acscatal.9b02305
ACS Catal. 2019, 9, 8213−8223

(VASP).[61,62] The exchange−correlation interactions were treated within the generalized gradient approximation of the Perdew−Burke−Ernzerhof (PBE) type.[63] Moreover, the electron wave functions were expanded by a plane wave cutoff of 400 eV, and a *k*-mesh of 5 × 5 × 1 was adopted to sample the Brillouin zone. Atomic relaxation was performed until all forces on each atom were <0.01 eV Å^{-1} and the convergence threshold for energy was 10^{-4} eV. The (7 × 7 × 1) supercell N-doped graphene was constructed by a periodic boundary condition, and the vacuum layers of 20 Å were set to be avoid periodic interaction. The van der Waals density functional approach was used to evaluate the effect of the van der Waals interaction.[64] The Bader charge analysis was performed to quantitatively estimate the amount of charge transfer.[65] The adsorption structures of Pt clusters searches were conducted by the CALYPSO package, using the particle swarm optimization algorithm.

■ ASSOCIATED CONTENT

Supporting Information

The Supporting Information is available free of charge on the ACS Publications website at DOI: 10.1021/acscatal.9b02305.

Supplementary methods, supported characterizations, DFT calculations, and additional electrochemical data (Figures S1−S28 and Tables S1−S7) (PDF)

■ AUTHOR INFORMATION

Corresponding Authors

*J. Z. e-mail: jczheng@csu.edu.cn.
*Z. J. e-mail: jiangzheng@sinap.ac.cn.
*F. P. e-mail: panfeng@pkusz.edu.cn.
*Z. L. e-mail:zhanlin@zju.edu.cn.

ORCID

Jiajun Tang: 0000-0002-0413-8862
Junchao Zheng: 0000-0002-7530-8590
Zheng Jiang: 0000-0002-0132-0319
Feng Pan: 0000-0002-8216-1339
Zhan Lin: 0000-0001-5009-8198

Author Contributions

$^{\nabla}$M.S., J.J., M.H., and M.W. contributed equally to this work.

Notes

The authors declare no competing financial interest.

■ ACKNOWLEDGMENTS

Z.L. thanks the funding supports of Zhejiang Province Science Fund for Distinguished Young Scholars (Project LR16B060001), Special Funds for Public Welfare Research and Capacity Building in Guangdong (Project 2017A010104024), and Key Technology and Supporting Platform of Genetic Engineering of Materials under State's Key Project of Research and Development Plan (Project 2016YFB0700600). J.Z. thanks the funding supports of National Natural Science Foundation of China (NSFC) (No. 51572300).

■ REFERENCES

(1) Sheng, W. C.; Gasteiger, H. A.; Shao-Horn, Y. Hydrogen Oxidation and Evolution Reaction Kinetics on Platinum: Acid Vs Alkaline Electrolytes. *J. Electrochem. Soc.* **2010**, *157*, B1529−B1536.

(2) Cheng, N. C.; Stambula, S.; Wang, D.; Banis, M. N.; Liu, J.; Riese, A.; Xiao, B. W.; Li, R. Y.; Sham, T. K.; Liu, L. M.; Botton, G. A.; Sun, X. L. Platinum Single-Atom and Cluster Catalysis of the Hydrogen Evolution Reaction. *Nat. Commun.* **2016**, *7*, 13638.

(3) Bu, L. Z.; Zhang, N.; Guo, S. J.; Zhang, X.; Li, J.; Yao, J. L.; Wu, T.; Lu, G.; Ma, J. Y.; Su, D.; Huang, X. Q. Biaxially Strained PtPb/Pt Core/Shell Nanoplate Boosts Oxygen Reduction Catalysis. *Science* **2016**, *354*, 1410−1414.

(4) Subbaraman, R.; Tripkovic, D.; Strmcnik, D.; Chang, K. C.; Uchimura, M.; Paulikas, A. P.; Stamenkovic, V.; Markovic, N. M. Enhancing Hydrogen Evolution Activity in Water Splitting by Tailoring Li+-Ni(OH)(2)-Pt Interfaces. *Science* **2011**, *334*, 1256−1260.

(5) Liang, S. X.; Hao, C.; Shi, Y. T. The Power of Single-Atom Catalysis. *ChemCatChem* **2015**, *7*, 2559−2567.

(6) Jones, J.; Xiong, H. F.; Delariva, A. T.; Peterson, E. J.; Pham, H.; Challa, S. R.; Qi, G. S.; Oh, S.; Wiebenga, M. H.; Pereira Hernandez, X. I. P.; Wang, Y.; Datye, A. K. Thermally Stable Single-Atom Platinum-on-Ceria Catalysts Via Atom Trapping. *Science* **2016**, *353*, 150−154.

(7) Escudero-Escribano, M.; Malacrida, P.; Hansen, M. H.; Vej-Hansen, U. G.; Velazquez-Palenzuela, A.; Tripkovic, V.; Schiotz, J.; Rossmeisl, J.; Stephens, I. E. L.; Chorkendorff, I. Tuning the Activity of Pt Alloy Electrocatalysts by Means of the Lanthanide Contraction. *Science* **2016**, *352*, 73−76.

(8) Stamenkovic, V. R.; Fowler, B.; Mun, B. S.; Wang, G. F.; Ross, P. N.; Lucas, C. A.; Markovic, N. M. Improved Oxygen Reduction Activity on Pt3Ni(111) Via Increased Surface Site Availability. *Science* **2007**, *315*, 493−497.

(9) Huang, X. Q.; Zhao, Z. P.; Cao, L.; Chen, Y.; Zhu, E. B.; Lin, Z. Y.; Li, M. F.; Yan, A. M.; Zettl, A.; Wang, Y. M.; Duan, X. F.; Mueller, T.; Huang, Y. High-Performance Transition Metal-Doped Pt3Ni Octahedra for Oxygen Reduction Reaction. *Science* **2015**, *348*, 1230−1234.

(10) Chen, C.; Kang, Y. J.; Huo, Z. Y.; Zhu, Z. W.; Huang, W. Y.; Xin, H. L. L.; Snyder, J. D.; Li, D. G.; Herron, J. A.; Mavrikakis, M.; Chi, M. F.; More, K. L.; Li, Y. D.; Markovic, N. M.; Somorjai, G. A.; Yang, P. D.; Stamenkovic, V. R. Highly Crystalline Multimetallic Nanoframes with Three-Dimensional Electrocatalytic Surfaces. *Science* **2014**, *343*, 1339−1343.

(11) Qian, H. F.; Jiang, D. E.; Li, G.; Gayathri, C.; Das, A.; Gil, R. R.; Jin, R. C. Monoplatinum Doping of Gold Nanoclusters and Catalytic Application. *J. Am. Chem. Soc.* **2012**, *134*, 16159−16162.

(12) Qiao, B. T.; Wang, A. Q.; Yang, X. F.; Allard, L. F.; Jiang, Z.; Cui, Y. T.; Liu, J. Y.; Li, J.; Zhang, T. Single-Atom Catalysis of Co Oxidation Using Pt-1/FeOx. *Nat. Chem.* **2011**, *3*, 634−641.

(13) Yang, X. F.; Wang, A. Q.; Qiao, B. T.; Li, J.; Liu, J. Y.; Zhang, T. Single-Atom Catalysts: A New Frontier in Heterogeneous Catalysis. *Acc. Chem. Res.* **2013**, *46*, 1740−1748.

(14) Zhang, W.; Zheng, W. T. Single Atom Excels as the Smallest Functional Material. *Adv. Funct. Mater.* **2016**, *26*, 2988−2993.

(15) Liu, J. Y. Catalysis by Supported Single Metal Atoms. *ACS Catal.* **2017**, *7*, 34−59.

(16) Nie, L.; Mei, D. H.; Xiong, H. F.; Peng, B.; Ren, Z. B.; Hernandez, X. I. P.; DeLariva, A.; Wang, M.; Engelhard, M. H.; Kovarik, L.; Datye, A. K.; Wang, Y. Activation of Surface Lattice Oxygen in Single-Atom Pt/CeO(2) for Low-Temperature CO Oxidation. *Science* **2017**, *358*, 1419.

(17) Yin, X. P.; Wang, H. J.; Tang, S. F.; Lu, X. L.; Shu, M.; Si, R.; Lu, T. B. Engineering the Coordination Environment of Single-Atom Platinum Anchored on Graphdiyne for Optimizing Electrocatalytic Hydrogen Evolution. *Angew. Chem., Int. Ed.* **2018**, *57*, 9382−9386.

(18) Li, X. G.; Bi, W. T.; Zhang, L.; Tao, S.; Chu, W. S.; Zhang, Q.; Luo, Y.; Wu, C. Z.; Xie, Y. Single-Atom Pt as Co-Catalyst for Enhanced Photocatalytic H-2 Evolution. *Adv. Mater.* **2016**, *28*, 2427−2431.

(19) Liu, J.; Jiao, M. G.; Lu, L. L.; Barkholtz, H. M.; Li, Y. P.; Wang, Y.; Jiang, L. H.; Wu, Z. J.; Liu, D. J.; Zhuang, L.; Ma, C.; Zeng, J.; Zhang, B. S.; Su, D. S.; Song, P.; Xing, W.; Xu, W. L.; Wang, Y.; Jiang, Z.; Sun, G. Q. High Performance Platinum Single Atom Electro-

DOI: 10.1021/acscatal.9b02305
ACS Catal. 2019, 9, 8213−8223

catalyst for Oxygen Reduction Reaction. *Nat. Commun.* **2017**, *8*, 15938.
(20) Wei, S. J.; Li, A.; Liu, J. C.; Li, Z.; Chen, W. X.; Gong, Y.; Zhang, Q. H.; Cheong, W. C.; Wang, Y.; Zheng, L. R.; Xiao, H.; Chen, C.; Wang, D. S.; Peng, Q.; Gu, L.; Han, X. D.; Li, J.; Li, Y. D. Direct Observation of Noble Metal Nanoparticles Transforming to Thermally Stable Single Atoms. *Nat. Nanotechnol.* **2018**, *13*, 856.
(21) von Weber, A.; Baxter, E. T.; Proch, S.; Kane, M. D.; Rosenfelder, M.; White, H. S.; Anderson, S. L. Size-Dependent Electronic Structure Controls Activity for Ethanol Electro-Oxidation at Pt-N/Indium Tin Oxide (N = 1 to 14). *Phys. Chem. Chem. Phys.* **2015**, *17*, 17601−17610.
(22) von Weber, A.; Anderson, S. L. Electrocatalysis by Mass-Selected Pt-N Clusters. *Acc. Chem. Res.* **2016**, *49*, 2632−2639.
(23) Guan, H. L.; Lin, J.; Qiao, B. T.; Yang, X. F.; Li, L.; Miao, S.; Liu, J. Y.; Wang, A. G.; Wang, X. D.; Zhang, T. Catalytically Active Rh Sub-Nanoclusters on TiO2 for Co Oxidation at Cryogenic Temperatures. *Angew. Chem., Int. Ed.* **2016**, *55*, 2820−2824.
(24) Dong, F.; Wu, L. W.; Sun, Y. J.; Fu, M.; Wu, Z. B.; Lee, S. C. Efficient Synthesis of Polymeric G-C3N4 Layered Materials as Novel Efficient Visible Light Driven Photocatalysts. *J. Mater. Chem.* **2011**, *21*, 15171−15174.
(25) Li, T. F.; Liu, J. J.; Song, Y.; Wang, F. Photochemical Solid-Phase Synthesis of Platinum Single Atoms on Nitrogen-Doped Carbon with High Loading as Bifunctional Catalysts for Hydrogen Evolution and Oxygen Reduction Reactions. *ACS Catal.* **2018**, *8*, 8450−8458.
(26) Liu, P. X.; Zhao, Y.; Qin, R. X.; Mo, S. G.; Chen, G. X.; Gu, L.; Chevrier, D. M.; Zhang, P.; Guo, Q.; Zang, D. D.; Wu, B. H.; Fu, G.; Zheng, N. F. Photochemical Route for Synthesizing Atomically Dispersed Palladium Catalysts. *Science* **2016**, *352*, 797−801.
(27) Fei, H. L.; Dong, J. C.; Feng, Y. X.; Allen, C. S.; Wan, C. Z.; Volosskiy, B.; Li, M. F.; Zhao, Z. P.; Wang, Y. L.; Sun, H. T.; An, P. F.; Chen, W. X.; Guo, Z. Y.; Lee, C.; Chen, D. L.; Shakir, I.; Liu, M. J.; Hu, T. D.; Li, Y. D.; Kirkland, A. I.; Duan, X. F.; Huang, Y. General Synthesis and Definitive Structural Identification of Mn4C4 Single-Atom Catalysts with Tunable Electrocatalytic Activities. *Nat. Catal.* **2018**, *1*, 63−72.
(28) Chen, W. X.; Pei, J. J.; He, C. T.; Wan, J. W.; Ren, H. L.; Zhu, Y. Q.; Wang, Y.; Dong, J. C.; Tian, S. B.; Cheong, W. C.; Lu, S. Q.; Zheng, L. R.; Zheng, X. S.; Yan, W. S.; Zhuang, Z. B.; Chen, C.; Peng, Q.; Wang, D. S.; Li, Y. D. Rational Design of Single Molybdenum Atoms Anchored on N-Doped Carbon for Effective Hydrogen Evolution Reaction. *Angew. Chem., Int. Ed.* **2017**, *56*, 16086−16090.
(29) Lin, Z. Y.; Waller, G.; Liu, Y.; Liu, M. L.; Wong, C. P. Facile Synthesis of Nitrogen-Doped Graphene Via Pyrolysis of Graphene Oxide and Urea, and Its Electrocatalytic Activity toward the Oxygen-Reduction Reaction. *Adv. Energy Mater.* **2012**, *2*, 884−888.
(30) Liao, G. Z.; Chen, S.; Quan, X.; Yu, H. T.; Zhao, H. M. Graphene Oxide Modified G-C3N4 Hybrid with Enhanced Photocatalytic Capability under Visible Light Irradiation. *J. Mater. Chem.* **2012**, *22*, 2721−2726.
(31) Williams, G.; Seger, B.; Kamat, P. V. TiO2-Graphene Nanocomposites. UV-Assisted Photocatalytic Reduction of Graphene Oxide. *ACS Nano* **2008**, *2*, 1487−1491.
(32) Duan, J. J.; Chen, S.; Jaroniec, M.; Qiao, S. Z. Porous C3N4 Nanolayers@N-Graphene Films as Catalyst Electrodes for Highly Efficient Hydrogen Evolution. *ACS Nano* **2015**, *9*, 931−940.
(33) Ruiz-Hitzky, E.; Darder, M.; Fernandes, F. M.; Zatile, E.; Palomares, F. J.; Aranda, P. Supported Graphene from Natural Resources: Easy Preparation and Applications. *Adv. Mater.* **2011**, *23*, 5250−5255.
(34) Eda, G.; Chhowalla, M. Chemically Derived Graphene Oxide: Towards Large-Area Thin-Film Electronics and Optoelectronics. *Adv. Mater.* **2010**, *22*, 2392−2415.
(35) Liang, Y. Y.; Li, Y. G.; Wang, H. L.; Zhou, J. G.; Wang, J.; Regier, T.; Dai, H. J. Co3O4 Nanocrystals on Graphene as a Synergistic Catalyst for Oxygen Reduction Reaction. *Nat. Mater.* **2011**, *10*, 780−786.
(36) Gao, G. P.; Jiao, Y.; Waclawik, E. R.; Du, A. J. Single Atom (Pd/Pt) Supported on Graphitic Carbon Nitride as an Efficient Photocatalyst for Visible-Light Reduction of Carbon Dioxide. *J. Am. Chem. Soc.* **2016**, *138*, 6292−6297.
(37) Wang, Y.; Wang, X. C.; Antonietti, M. Polymeric Graphitic Carbon Nitride as a Heterogeneous Organocatalyst: From Photochemistry to Multipurpose Catalysis to Sustainable Chemistry. *Angew. Chem., Int. Ed.* **2012**, *51*, 68−89.
(38) Bulushev, D. A.; Zacharska, M.; Lisitsyn, A. S.; Podyacheva, O. Y.; Hage, F. S.; Ramasse, Q. M.; Bangert, U.; Bulusheva, L. G. Single Atoms of Pt-Group Metals Stabilized by N-Doped Carbon Nanofibers for Efficient Hydrogen Production from Formic Acid. *ACS Catal.* **2016**, *6*, 3442−3451.
(39) Wenderich, K.; Mul, G. Methods, Mechanism, and Applications of Photodeposition in Photocatalysis: A Review. *Chem. Rev.* **2016**, *116*, 14587−14619.
(40) Tang, Y. N.; Yang, Z. X.; Dai, X. Q. Preventing the CO Poisoning on Pt Nanocatalyst Using Appropriate Substrate: A First-Principles Study. *J. Nanopart. Res.* **2012**, *14*, 844.
(41) Bruix, A.; Lykhach, Y.; Matolinova, I.; Neitzel, A.; Skala, T.; Tsud, N.; Vorokhta, M.; Stetsovych, V.; Sevcikova, K.; Myslivecek, J.; Fiala, R.; Vaclavu, M.; Prince, K. C.; Bruyere, S.; Potin, V.; Illas, F.; Matolin, V.; Libuda, J.; Neyman, K. M. Maximum Noble-Metal Efficiency in Catalytic Materials: Atomically Dispersed Surface Platinum. *Angew. Chem., Int. Ed.* **2014**, *53*, 10525−10530.
(42) Geerlings, P.; De Proft, F.; Langenaeker, W. Conceptual Density Functional Theory. *Chem. Rev.* **2003**, *103*, 1793−1873.
(43) Wang, J.; Huang, Z. Q.; Liu, W.; Chang, C. R.; Tang, H. L.; Li, Z. J.; Chen, W. X.; Jia, C. J.; Yao, T.; Wei, S. Q.; Wu, Y.; Li, Y. D. Design of N-Coordinated Dual-Metal Sites: A Stable and Active Pt-Free Catalyst for Acidic Oxygen Reduction Reaction. *J. Am. Chem. Soc.* **2017**, *139*, 17281−17284.
(44) Zhang, Z. L.; Zhu, Y. H.; Asakura, H.; Zhang, B.; Zhang, J. G.; Zhou, M. X.; Han, Y.; Tanaka, T.; Wang, A. Q.; Zhang, T.; Yan, N. Thermally Stable Single Atom Pt/M-Al2O3 for Selective Hydrogenation and Co Oxidation. *Nat. Commun.* **2017**, *8*, 16100.
(45) Dai, Y.; Gorey, T. J.; Anderson, S. L.; Lee, S.; Lee, S.; Seifert, S.; Winans, R. E. Inherent Size Effects on Xanes of Nanometer Metal Clusters: Size Selected Platinum Clusters on Silica. *J. Phys. Chem. C* **2017**, *121*, 361−374.
(46) Zhao, S. L.; Wang, Y.; Dong, J. C.; He, C. T.; Yin, H. J.; An, P. F.; Zhao, K.; Zhang, X. F.; Gao, C.; Zhang, L. J.; Lv, J. W.; Wang, J. X.; Zhang, J. Q.; Khattak, A. M.; Khan, N. A.; Wei, Z. X.; Zhang, J.; Liu, S. Q.; Zhao, H. J.; Tang, Z. Y. Ultrathin Metal-Organic Framework Nanosheets for Electrocatalytic Oxygen Evolution. *Nat. Energy* **2016**, *1*, 16184.
(47) Yi, S. S.; Yan, J. M.; Wulan, B. R.; Li, S. J.; Liu, K. H.; Jiang, Q. Noble-Metal-Free Cobalt Phosphide Modified Carbon Nitride: An Efficient Photocatalyst for Hydrogen Generation. *Appl. Catal., B* **2017**, *200*, 477−483.
(48) Kibsgaard, J.; Jaramillo, T. F.; Besenbacher, F. Building an Appropriate Active-Site Motif into a Hydrogen-Evolution Catalyst with Thiomolybdate Mo3S13 (2-) Clusters. *Nat. Chem.* **2014**, *6*, 248−253.
(49) Chen, W. F.; Wang, C. H.; Sasaki, K.; Marinkovic, N.; Xu, W.; Muckerman, J. T.; Zhu, Y.; Adzic, R. R. Highly Active and Durable Nanostructured Molybdenum Carbide Electrocatalysts for Hydrogen Production. *Energy Environ. Sci.* **2013**, *6*, 943−951.
(50) Zhang, C. H.; Sha, J. W.; Fei, H. L.; Liu, M. J.; Yazdi, S.; Zhang, J. B.; Zhong, Q. F.; Zou, X. L.; Zhao, N. Q.; Yu, H. S.; Jiang, Z.; Ringe, E.; Yakobson, B. I.; Dong, J. C.; Chen, D. L.; Tour, J. M. Single-Atomic Ruthenium Catalytic Sites on Nitrogen-Doped Graphene for Oxygen Reduction Reaction in Acidic Medium. *ACS Nano* **2017**, *11*, 6930−6941.
(51) Wang, J.; Xu, F.; Jin, H. Y.; Chen, Y. Q.; Wang, Y. Non-Noble Metal-Based Carbon Composites in Hydrogen Evolution Reaction: Fundamentals to Applications. *Adv. Mater.* **2017**, *29*, 1605838.
(52) Li, Y. G.; Wang, H. L.; Xie, L. M.; Liang, Y. Y.; Hong, G. S.; Dai, H. J. MoS2 Nanoparticles Grown on Graphene: An Advanced

DOI: 10.1021/acscatal.9b02305
ACS Catal. 2019, 9, 8213−8223

Catalyst for the Hydrogen Evolution Reaction. *J. Am. Chem. Soc.* **2011**, *133*, 7296−7299.
(53) Strmcnik, D.; Lopes, P. P.; Genorio, B.; Stamenkovic, V. R.; Markovic, N. M. Design Principles for Hydrogen Evolution Reaction Catalyst Materials. *Nano Energy* **2016**, *29*, 29−36.
(54) Kecsenovity, E.; Endrodi, B.; Toth, P. S.; Zou, Y.; Dryfe, R. A. W.; Rajeshwar, K.; Janaky, C. Enhanced Photoelectrochemical Performance of Cuprous Oxide/Graphene Nanohybrids. *J. Am. Chem. Soc.* **2017**, *139*, 6682−6692.
(55) Lightcap, I. V.; Kosel, T. H.; Kamat, P. V. Anchoring Semiconductor and Metal Nanoparticles on a Two-Dimensional Catalyst Mat. Storing and Shuttling Electrons with Reduced Graphene Oxide. *Nano Lett.* **2010**, *10*, 577−583.
(56) Lv, J.; Wang, Y. C.; Zhu, L.; Ma, Y. M. Particle-Swarm Structure Prediction on Clusters. *J. Chem. Phys.* **2012**, *137*, 084104.
(57) Wang, D. S.; Gao, Y.; Liu, Y. H.; Gogotsi, Y.; Meng, X.; Chen, G.; Wei, Y. J. Investigation of Chloride Ion Adsorption onto Ti2C Mxene Monolayers by First-Principles Calculations. *J. Mater. Chem. A* **2017**, *5*, 24720−24727.
(58) Norskov, J. K.; Bligaard, T.; Logadottir, A.; Kitchin, J. R.; Chen, J. G.; Pandelov, S.; Stimming, U. Trends in the Exchange Current for Hydrogen Evolution. *J. Electrochem. Soc.* **2005**, *152*, J23−J26.
(59) Li, H.; Tsai, C.; Koh, A. L.; Cai, L. L.; Contryman, A. W.; Fragapane, A. H.; Zhao, J. H.; Han, H. S.; Manoharan, H. C.; Abild-Pedersen, F.; Norskov, J. K.; Zheng, X. L. Activating and Optimizing MoS2 Basal Planes for Hydrogen Evolution through the Formation of Strained Sulphur Vacancies. *Nat. Mater.* **2016**, *15*, 48.
(60) Mahmood, J.; Li, F.; Jung, S. M.; Okyay, M. S.; Ahmad, I.; Kim, S. J.; Park, N.; Jeong, H. Y.; Baek, J. B. An Efficient and Ph-Universal Ruthenium-Based Catalyst for the Hydrogen Evolution Reaction. *Nat. Nanotechnol.* **2017**, *12*, 441−446.
(61) Kresse, G.; Furthmuller, J. Efficiency of Ab-Initio Total Energy Calculations for Metals and Semiconductors Using a Plane-Wave Basis Set. *Comput. Mater. Sci.* **1996**, *6*, 15−50.
(62) Kresse, G.; Furthmuller, J. Efficient Iterative Schemes for Ab Initio Total-Energy Calculations Using a Plane-Wave Basis Set. *Phys. Rev. B: Condens. Matter Mater. Phys.* **1996**, *54*, 11169−11186.
(63) Perdew, J. P.; Chevary, J. A.; Vosko, S. H.; Jackson, K. A.; Pederson, M. R.; Singh, D. J.; Fiolhais, C. Atoms, Molecules, Solids, and Surfaces - Applications of the Generalized Gradient Approximation for Exchange and Correlation. *Phys. Rev. B: Condens. Matter Mater. Phys.* **1992**, *46*, 6671−6687.
(64) Grimme, S.; Antony, J.; Ehrlich, S.; Krieg, H. A Consistent and Accurate Ab Initio Parametrization of Density Functional Dispersion Correction (Dft-D) for the 94 Elements H-Pu. *J. Chem. Phys.* **2010**, *132*, 154104.
(65) Henkelman, G.; Arnaldsson, A.; Jonsson, H. A Fast and Robust Algorithm for Bader Decomposition of Charge Density. *Comput. Mater. Sci.* **2006**, *36*, 354−360.

DOI: 10.1021/acscatal.9b02305
ACS Catal. 2019, 9, 8213−8223